

Numerical Investigation of Jet Interaction in a Supersonic Freestream

Houshang B. Ebrahimi

ATA, Inc., Arnold Air Force Base, Tennessee 37389

DOI: 10.2514/1.29847

The objective of this investigation is to numerically evaluate effects of a reaction control (divert) jet on the aerodynamic performance of a generic interceptor missile operating at supersonic flight conditions. The effects investigated include transient operation, external chemical reactions and combustion, and geometric scale, specifically full scale versus subscale. Parametric computational fluid dynamic solutions are obtained at altitude conditions corresponding to 19.7 km for the following scenarios: 1) steady-state conditions with the lateral control jet turned off; 2) steady-state conditions with the lateral control jet turned on; 3) steady-state conditions with the lateral control jet turned off, one-tenth subscale geometry; 4) steady-state conditions with the lateral control jet turned on, one-tenth subscale geometry; 5) transient jet startup conditions; 6) transient jet shutdown conditions; 7) steady-state, finite-rate chemistry; and 8) steady-state, chemically frozen calculations. Specifically, all chemical reactions are “turned off.” Vehicle forces and moments are assessed for each solution by integrating the computed surface pressures and viscous shear stresses on the missile surfaces. These results are used to determine the influence of the jet interaction effects on the transient, external combustion, and geometric scale and associated effects on the aerodynamic performance of the missile. The analysis predicts strong transient influences, small external combustion influences, and very small full-scale vs one-tenth subscale geometry effects on the integrated normal force and pitching moment.

Nomenclature

A_{ref}	= reference area
C_r	= jet thrust ratio
C_x, C_n, C_M	= axial, normal, and moment coefficients
D	= diameter of missile, m
F_j	= force produced at the jet exit
F_{ji}	= jet interaction force
F_x	= surface-integrated force component
K	= jet amplification factor
L	= length of missile, m
M	= freestream Mach number
M_w	= molecular weight
P	= static pressure, atm
P_{oj}	= stagnation pressure, divert jet, Pa
q	= dynamic head; $0.5\rho_\infty V_\infty^2$
S	= cylinder cross-sectional area, m^2
T	= static temperature, K
T_{oj}	= stagnation temperature, divert jet, K
T_t	= jet thrust, N
V_∞	= freestream velocity
γ	= ratio of specific heats
ρ_∞	= freestream density

Subscripts

inf	= freestream condition
jet	= condition with jet
no jet	= condition with no jet

I. Introduction

THE flowfield resulting from the interaction of a side (lateral) jet injected into a supersonic external flow is called the jet interaction (JI) flowfield. The flowfield produced by a jet exhausting into a crossflow is a complex fluid dynamics phenomenon which occurs commonly in military and commercial applications. Examples of applications of the jet interaction principles range from the very low-speed regimes of a chimney plume in a crossflow to the very high speed of scramjet combustion and hypersonic missile control systems. Computational fluid dynamic (CFD) simulations of the physical phenomenon occurring when a gas is injected into a crossflow includes several challenging aspects, including the yaw and the pitch angles of the injector and the flow conditions of the jet (subsonic, choked, or supersonic), as well as the freestream conditions (subsonic, supersonic, laminar, or turbulent), not to mention the chemical composition of the gases based on various assumptions including perfect gas, single or multiple phase, nonreacting mixture, reacting mixture, etc. A schematic of the underexpanded transverse injection flowfield appears in Fig. 1. This illustration describes the qualitative features of the injection flowfield when the supersonic crossflow is displaced by the fuel jet as if a bluff body were inserted into the flow. As a result, a three-dimensional bow shock is formed upstream of the injector exit, causing the upstream wall boundary layer to separate. In the separation region, the boundary layer and jet fluids mix subsonically upstream of the jet exit. This region is important in transverse injection because of its flame-holding capability in combusting situations. In fact, the jet interaction shock structure and flowfield are highly analogous to those created by a forward-facing step.

The heart of a missile is its body, which is equivalent to the fuselage of an aircraft. The missile body contains the guidance and control system, warhead, and propulsion system. Some missiles may consist of only the body, but most have additional surfaces that generate lift and provide maneuverability. Depending on the source, these surfaces are referred to by various names. In particular, many sources use the generic term, “fin,” to refer to any aerodynamic surface on a missile. Missile designers, however, are more precise in their naming methodology and generally consider these surfaces to fall into three major categories: canards, wings, and tail fins.

To complete its mission successfully, a missile defense interceptor must be highly maneuverable as it travels at supersonic or hypersonic

Presented as Paper 4866 at the 2005 Arizona Joint Propulsion and Power Conference, Tucson, AZ, 16–22 July 2005; received 18 January 2007; revision received 15 May 2007; accepted for publication 23 May 2007. Copyright © 2007 by the American Institute of Aeronautics and Astronautics, Inc. The U.S. Government has a royalty-free license to exercise all rights under the copyright claimed herein for Governmental purposes. All other rights are reserved by the copyright owner. Copies of this paper may be made for personal or internal use, on condition that the copier pay the \$10.00 per-copy fee to the Copyright Clearance Center, Inc., 222 Rosewood Drive, Danvers, MA 01923; include the code 0022-4650/08 \$10.00 in correspondence with the CCC.

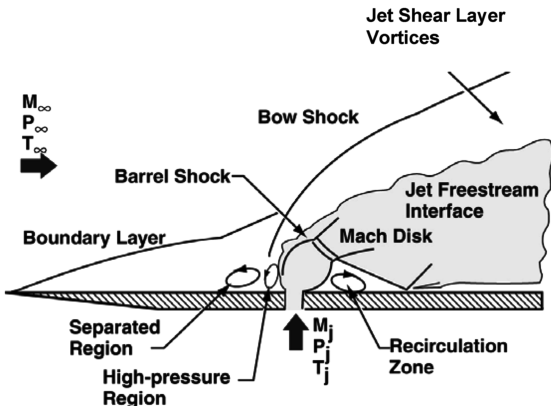


Fig. 1 Schematic of the underexpanded transverse injection JI flowfield.

speeds. Quick-response maneuverability, especially during the end-game phase of the interceptor's mission, is achieved by a rapid airframe response time to the attitude control system guidance. Surface-mounted, fast-reacting, lateral-jet control thrusters issuing at large angles relative to the interceptor's direction of flight offer an effective supplement to conventional aerodynamic control surfaces. These jets provide the required response times and improve the missile's agility and maneuverability when compared with fin surfaces.

The mutual interference of the control jet-thruster exhaust with the supersonic freestream leads to thrust and moment amplifications, relative to the aerodynamic effect of the jet thrust alone, because of high-pressure regions that form upstream of the jet on the missile surface. These high-pressure regions are created by the shock structure that develops in the supersonic freestream in front of the lateral jet. Large regions of separated flow created by the missile boundary-layer interactions with the shock structure cause the high-pressure areas to increase in size. This effect amplifies the response of the divert jets. Effective exploitation of this effect can lead to improved effectiveness of the missile interceptor. Insight into this phenomenon is necessary because, at some missile orientations and flow conditions, the mutual interference of the jet-thruster flowfield with the freestream leads to "deamplification" (i.e., negative effects on the missile). Therefore, an understanding of the controlling factors that produce thrust amplification, as well as of those that produce thrust deamplification, is critical to developing a credible design basis for optimal missile aerodynamic performance [1,2]. The JI phenomena and the effect of the jet plume on the surfaces pressure distribution downstream of the jet exit, which is not discussed here, are described in [1–4]. The ability of ground test facilities to fully duplicate flight conditions is very limited. Limitations include test duration, test section and core-flow area, and flow quality (i.e., freestream flow nonuniformity and angularity). Because of these limitations, the relationship between the jet behavior in a ground test and the jet behavior in flight continues to be an unresolved issue. Areas of uncertainty arise when only ground test data are used to develop a prediction methodology for high-speed flight JI flowfields. Simulation issues include hot-jet versus cold-jet effects, chemically reacting versus nonreacting jet conditions, transient phenomena, geometric scale, and missile-maneuvering considerations. It is still uncertain if a cold-flow ground facility (i.e., low-enthalpy freestream) can accurately simulate the required conditions and provide JI ground test data that can be used to predict missile performance in the actual flight environment.

The operation of a divert-jet control thruster is a time-dependent event. This time dependency may be described as a ramp-up interval in which the jet transitions from quiescence to full thrust, followed by a relatively steady-state time interval at full thrust conditions, followed by a jet-tail off time interval in which the jet thrust decays from full thrust back to quiescence conditions. Typically, this complete duty cycle is on the order of milliseconds, during which time the flowfield environment and, consequently, the interceptor

missile, responds to the jet. However, most CFD methodologies assume a steady full-on jet and compute a corresponding steady-state solution, ignoring the transient effects. Predictions from these CFD analyses are probably not adequate for control system design purposes or for comparison to ground tests in which a complete jet duty cycle is included.

CFD calculations offer the potential to predict complex JI flowfields and to reduce, and sometimes eliminate, the uncertainties associated with ground test simulations. CFD solutions could be used to locate test instrumentation, optimize the test matrix, select the ground test facility most appropriate for a particular kind of JI test, and to supplement an experimental database for developing improved performance prediction methodologies.

Previous CFD solutions published by the author [5] demonstrate the potential to numerically simulate complex, three-dimensional JI flowfields and assess the influence of the transient, external combustion, and geometric scale JI effects on the aerodynamic performance of the interceptor missile. In addition, just as JI phenomena pose a challenge for ground test simulations, JI effects also present a formidable problem for adequate numerical simulations.

The ability of ground test facilities to adequately reproduce the external combustion of fuel-rich jet exhaust gases which occur in flight is a significant concern affecting the utility of ground test measurements in assessing control/divert-jet operation and performance. Further, combustion occurring within ground test facility test sections significantly increases risk factors associated with the test, as does environmental contamination created by the combustion products.

Reference [3] includes validation results of the CFD methodology used in this investigation obtained for steady-state JI conditions. The validation is based on quantitative comparisons of the CFD results with ground test measurements. The validation results indicate reasonable agreement is achieved when comparing the CFD computations with steady-state ground test JI measurements. Similar CFD solutions can be obtained for transient JI conditions. However, validations of the transient calculations are currently not possible because resolved transient measurements are not available for comparisons with the CFD results. Presently, transient CFD calculations are compared to qualitatively assess JI design features that are known to impact interceptor performance.

The purpose of this computational effort is to investigate potential issues impacting the design and development of a missile defense interceptor. These issues are evaluated by comparisons of computed missile aerodynamic performance characteristics assuming the following JI conditions: steady-state versus transient conditions; external chemical combustion versus frozen chemistry conditions, and subscale versus full-scale geometry.

Because of the complexity of these phenomena and associated ground test limitations in simulating the free flight environment, computational results provide insight needed for pretest planning and are also useful for posttest data analysis. For example, the design of a JI ground test requires a priori knowledge of how far the jet is expected to extend from the missile body at each freestream condition within the test matrix to determine if the jet will impinge on the test section walls. For transient JI ground tests, the ability of the ground test facility to sustain the test conditions needed for a full control jet-thruster duty cycle can be evaluated using a transient CFD solution. As CFD methods to predict JI flowfields mature and more measurements become available for CFD validation, the uncertainties of interceptor performance prediction methodologies will continue to decrease.

II. Computational Validation for JI Applications

Numerical solutions of the flow interactions occurring when divert jets penetrate into freestream flows are challenging because the transverse jet produces a complex region of 3-D separated flow. Whenever a secondary flow is injected into a supersonic primary stream, the secondary flow acts as an obstacle, inducing a strong bow shock located upstream of the injector location. This bow shock

wave interacts with the missile body boundary layer allowing the pressure in the separated region to propagate through the boundary layer upstream of the shock, producing a boundary-layer separation region.

This complex JI flowfield phenomenon has been simulated using the general propulsion analysis chemical kinetic and two-phase CFD code (GPACT). The GPACT numerical methodology is described in detail in [3,5–7]. The GPACT numerical scheme used a structured, multiblock grid in CFD solution of the Reynolds averaged Navier–Stokes (RANS) equations. GPACT is applicable to compressible flowfields for Mach number flow conditions equal to 0.1 and greater. The solution incorporates options for finite-rate, kinetic chemistry or equilibrium chemistry and is appropriate for most chemical propulsion applications. GPACT also includes options for steady and time-accurate simulations. The governing equations are formulated by means of a finite volume numerical technique and discretized using an upwind scheme. The conservation equations are coupled with the convection and diffusion of the chemical species and the reaction source terms to consider the transportation and mixture of chemical species. As such, GPACT is based on a sophisticated numerical algorithm which is used to solve coupled flow equations including conservation, two-phase flow, and sophisticated chemical approximations for complex three-dimensional geometry and flow phenomena.

To validate the GPACT model for JI applications, GPACT was used to simulate 3-D divert-jet interactions with freestream interaction effects for two cases for which experimental data have been acquired. Both validation cases include a lateral divert jet. The computations are completed for the specified geometries and test conditions at which wind-tunnel JI experiments were conducted and associated JI flowfield measurements obtained. The computed flowfield results from GPACT are compared with wind-tunnel experimental data as a validation of the GPACT model for JI applications. The scope of this initial validation does not consider grid sensitivities.

The first validation case includes a biconic missile geometry with a lateral divert jet located downstream on the missile body [3,8]. The

leading cone half-angle is 10.4 deg, and the trailing cone half-angle is 6 deg, as noted in Fig. 2. The lateral jet is located 0.455 m aft of the virtual nose on the 10.4 deg trailing cone surface. The centerline of the jet is oriented normal to the cone centerline in the vertical plane. The biconic section has a 0-degree angle of attack with respect to the freestream. The freestream flow conditions are specified as Mach number equal to 9.7, static temperature equal to 61 K, static pressure equal to 523 Pa, and density equal to 0.025 kg/m³. The freestream flow is composed of air. The divert jet is composed of nitrogen, injected vertically at Mach 2, with a corresponding static pressure of 10,000 Pa and a density of 2.2 kg/m³.

GPACT solutions were obtained for the specified geometry and wind-tunnel test conditions, with and without operation of the lateral divert jet [3]. Figure 3a compares calculated and experimental nondimensional pressure values on the missile surface. The body surface pressures presented in Fig. 3 are normalized by the freestream pressure value. The initial high-pressure value which results from the detached bow shock is captured by the GPACT calculation along with the downstream pressure rise associated with the boundary-layer separation and the subsequent reattachment (or the recompression shock) created by the body geometry. The experimental measurements do not capture the initial high-pressure value resulting from the separation behind the bow shock. This is likely due to the placement of the pressure measurement taps on the body which did not include the region near the nose. This comparison demonstrates the utility of CFD solutions in pretest planning and optimization of measurement positions. The CFD pressures calculated along the body surface for the case without the divert jet operating agree reasonably well with measured data [3]. In Fig. 3b, the GPACT solution is compared with measurements obtained when the divert jet was in operation. The agreement noted between the calculations and the measurements is favorable. In this case, the GPACT calculation captures the behavior of the measurements within the shock region created by the lateral-jet penetration into the freestream. The pressure behavior within the resulting boundary-layer separation zone along the body upstream of the injection point is also captured by the GPACT model. The CFD solution provides

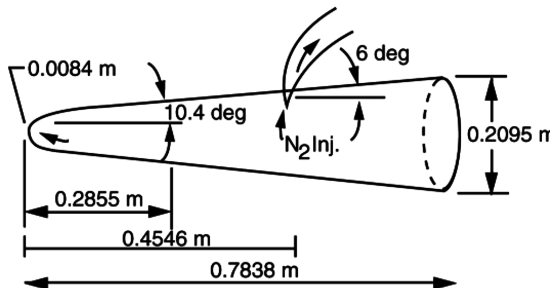


Fig. 2 Biconic case 1 geometry and flow conditions.

Test Conditions		
	Freestream	Nitrogen
Pressure, Pa	523	10,000
Density, Kg/m ³	0.025	2.2
Mach No.	9.7	2.0

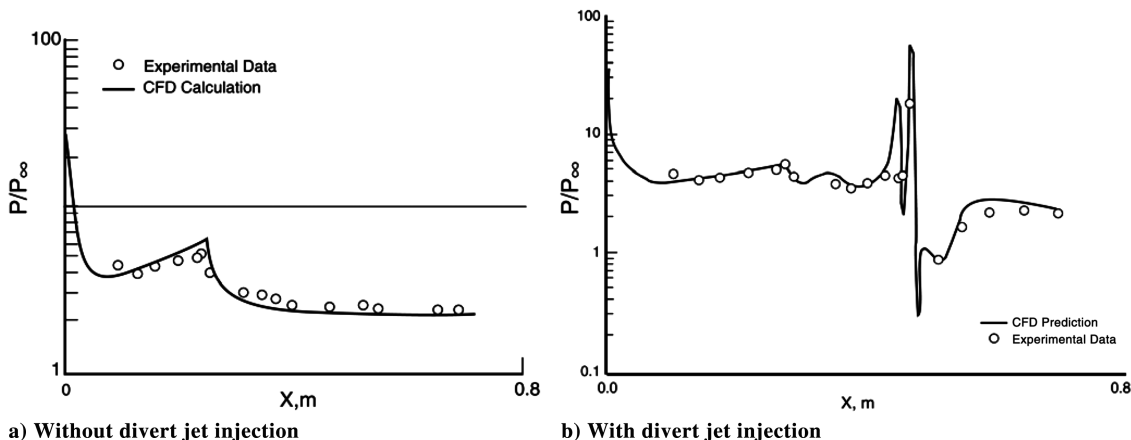


Fig. 3 Comparisons of measured and calculated surface pressure distributions, with and without divert-jet injections.

Table 1 Experimental and numerical normal force coefficient comparison

Test case	Jet thrust ratio, C_r	Angle of attack, deg	Divert-jet location	Normal thrust coefficient, measured, C_n	Normal thrust coefficient, calc. C_n
1	1.0	20	Leeward jet	3.37	3.25
2	1.0	20	Windward jet	4.64	4.58
3	4.0	20	Leeward jet	0.21	0.23
4	4.0	20	Windward jet	7.33	7.28
5	Jet off	20	No jet	4.36	4.20

spatial resolution in this region sufficient to resolve the pressure peak values on the body which are not totally resolved by the spatial resolution of the measurement pressure tap locations.

The second validation case includes a three-dimensional missile shape operating at angle of attack, including a lateral divert jet. The GPACT results for this case are compared with the results of other calculations and with wind-tunnel experimental data acquired by Srivastava [9]. The wind-tunnel freestream conditions at which measurements were obtained are specified as Mach number equal to 2.97 and Reynolds numbers equal to 8.2×10^5 . The flow conditions and comparisons of measured and calculated normal thrust coefficient values are summarized in Table 1 for the five cases considered. For all five cases, the angle of attack is specified to be 20 deg. The ratio of the divert-jet thrust to the freestream thrust values, $C_r (T_j/q^* s)$ is equal to 1 for cases 1 and 2, and is equal to 4 for cases 3 and 4. The measured normal thrust coefficient is the figure of merit compared with the calculated values in Table 1.

Comparisons of the measured and computed normal force C_n are shown in Table 1. The overall comparisons between the CFD predictions and experimental measurements are reasonable. The CFD results duplicate the trend behavior noted in the measurements. A detailed discussion of this validation case and the thrust coefficient comparisons presented in Table 1 is provided in [1]. The results of the validation cases indicate GPACT is a proficient and reasonable CFD analysis model for JI flow simulations and analysis.

III. Approach and Analysis

This investigation consists of computational simulations of JI flowfield behavior, including calculations of the forces and moments at freestream flight conditions at 19.7 km (64,500 ft) altitude, Mach number 5, and Reynolds number 3.0×10^6 . The interceptor missile is equipped with a lateral control jet for guidance. The objective of the computational effort is to investigate the effects of the divert jet occurring between transient startup and shutdown and compare with the results obtained assuming steady-state operations. In addition, flowfield solutions that account for external chemical combustion occurring in the exhaust plume are compared with solutions assuming nonreacting flow conditions. Finally, effects of full-scale vs one-tenth subscale geometry are considered.

Identical geometry specifications for the missile and divert thruster are maintained for all simulations. The generic missile geometry, shown in Fig. 4, is a long, slender missile body design, $L/D = 14.5$, including forward and aft fins. The generic missile consists of four rectangular dorsal fins and tail fins. This geometry is representative of interceptor designs and is selected because divert-thruster transient effects are suspected to be influenced by the presence of fins on the missile. For each dorsal fin, the leading edge is located five calibers (1 caliber = 1 diameter = 13.4 in. = 34.3 cm) from the nose tip and measures 0.5 calibers in span and five calibers in chord. Similarly, each tail fin begins 13 calibers from the nose tip and measures 0.5 calibers in span and one caliber in chord. The single jet-thruster exit centerline is located 45 deg circumferentially between the dorsal fins and six calibers downstream from the nose tip. The diameter of the divert-jet exit is 2.96 in. (7.53 cm).

The missile freestream Mach number is maintained at 5.0. The Mach number at the exit of the diverging divert-thruster's nozzle is nominally 3 (calculated on the basis of chamber conditions). A thermally and calorically perfect gas ($\gamma = 1.4$ for freestream and 1.3 for divert jet) was assumed in the CFD simulation in contrasting transient vs steady-state, full- vs one-tenth scale geometric

considerations. Finite-rate chemistry effects are numerically investigated using a chemical system consisting of 14 species; specifically, H, O, OH, H₂, H₂O, CO, CO₂, O₂, C, N₂, HCl, Cl, H₂O₂, and HO₂ and 46 reactions. CFD solutions that incorporate the chemical kinetic model are compared with solutions assuming chemically frozen conditions. The angle of attack of the interceptor is specified as 0 deg. For all calculations the divert jet is maintained at the same position on the interceptor missile with its nozzle axis situated at 90 deg to the thrust vector of the interceptor for all simulations.

The divert jet is located between two of the dorsal fins positioned at the center of gravity for the interceptor missile. The divert-jet thrust chamber consists of a converging/diverging nozzle geometry, and stagnation conditions specified such that the nominal Mach number at the nozzle exit is equal to 3.0. The divert-jet internal flow regime is included within the computational domain. The stagnation conditions specified for the divert thruster are specified as

$$P_{oj} = 176 \text{ atm} \quad T_{oj} = 2278 \text{ K}$$

Transient CFD flowfield solutions are completed to assess the transient effects of the divert-thruster startup and shutdown processes. CFD solutions are also completed to simulate the flowfield surrounding the interceptor missile body with the divert thruster present on the interceptor body, but not operating. These solutions indicate that even when the divert jet is turned off, the presence of the divert-jet cavity on the missile body influences the missile aerodynamic performance. Detailed CFD solutions for eight transient cases are provided in [5].

Two cases were simulated at full-scale and one-tenth scale geometry to contrast the effects of the geometric scale on the aerodynamic performance at supersonic flight conditions. In evaluation of the geometric scale effects, a two-species (freestream and jet) nonreacting CFD calculation is completed allowing the mixing between the freestream and the divert jet, without combustion.

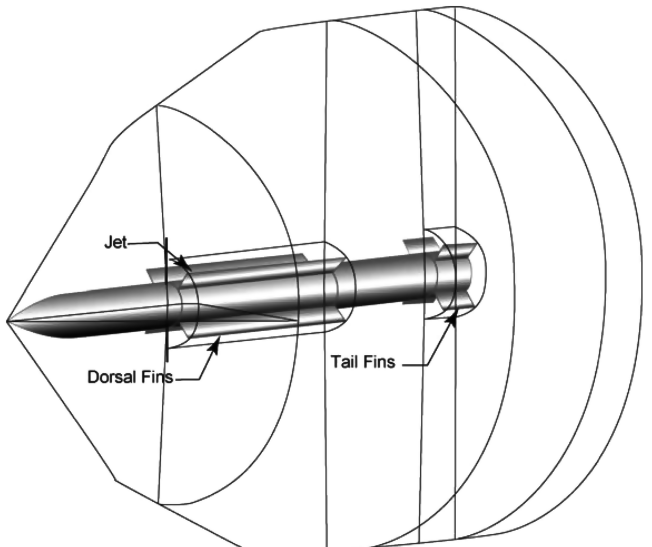


Fig. 4 Surface definition showing missile geometry and computational zones.

The effects of combustion occurring in the divert thruster exhaust plume flowfield on the aerodynamic interceptor forces and moments are evaluated by contrasting nonreacting and reacting CFD JI solutions. Calculations are performed with chemical reactions “turned off” (frozen flow) and with fully active finite-rate chemistry included in the solution process. Both the reacting and nonreacting solutions exhibit similar flowfield phenomena, structure, and features. The pressure fields for the solutions with and without chemistry are integrated over the vehicle surface to determine the forces and moments. All moment calculations are performed with respect to a point on the vehicle centerline six calibers from the nose tip. This axial position corresponds to the center of the jet exit area. The forces and moment coefficients are compared. These calculations indicate that external burning in the divert-jet exhaust produces a noticeable, but small effect on the forces and moments experienced by this type of vehicle, including an increased thrust amplification for the reacting case.

IV. Results and Discussion

As noted earlier, GPACT solutions of the three-dimensional viscous Navier-Stokes equations (Reynolds average) with a $k-\varepsilon$ turbulence model were completed to evaluate JI effects. Forces and moments on the missile body were determined by integrating the surface pressures and viscous shear stresses over the entire surface of the missile. Forces associated with interceptor base entrainment are not considered. Divert-jet thrust was obtained by integrating calculated flux across the jet nozzle exit diameter. The results show significant interactions of the jet-induced flowfield with the missile fin surfaces, which produce additional effects, when compared with the body only results.

Flowfield results obtained at the 19.7-km (64,500 ft) altitude assuming steady-state, jet-on conditions are shown in Fig. 5. Mach number profiles at four axial locations on the missile body are presented. The axial locations include 1) just downstream of the divert-jet exit location; 2) at the end of the dorsal fins; 3) halfway between the divert nozzle exit and the trailing edge of the dorsal fins; and 4) at the end of the missile. The behavior of the underexpanded divert jet is noted by the rapid divergence of the jet exhaust shown in the first cross-section location just downstream of the divert-jet exit. Effects of the divert-jet and freestream interactions are noticeable in all Fig. 5 results. Note the high-pressure (i.e., low Mach number) interaction region impinging on the fins in Fig. 5.

The large circulation bubble created by the freestream interaction with the divert-jet plume is evident in the region upstream of the divert nozzle exit. The formation of a secondary separation region is also apparent. These recirculation zones create a high-pressure region and an associated force on the missile surface. The force exerted by the recirculation modifies the divert jet's thrust force and influences the moment about the center of gravity of the interceptor missile. As indicated in Fig. 6, a separation region on the upstream side of the divert jet is evident. A separation region is also present on the downstream side, creating an expansion region.

The freestream conditions and description of the individual cases for flowfield calculations for each case are listed in Tables 2 and 3, respectively. Case 2 represents the baseline case at full-scale flight conditions. Case 4 simulates wind-tunnel conditions at one-tenth scale. Comparisons of the computation for these two cases will constitute the geometric scaling analysis. Note that all of the cases are at a freestream Mach number of 5 and 0 angle of attack. Also, because the freestream flow conditions are the same for cases 1–4, unit Reynolds number is matched, which goes against conventional wisdom for matching Reynolds number. The reason for this choice is that producing flight Reynolds number is often impossible in current wind tunnels. Moreover, normal force and pitching moment receive the highest priority for reducing the missile response time and are less sensitive to Reynolds number effects than is axial force, which is secondary in significance for jet interactions.

The force and moment coefficients, C_x and C_M , are defined as

$$C_x = F_x / 0.5 \rho_\infty V_\infty^2 A_{\text{ref}}$$

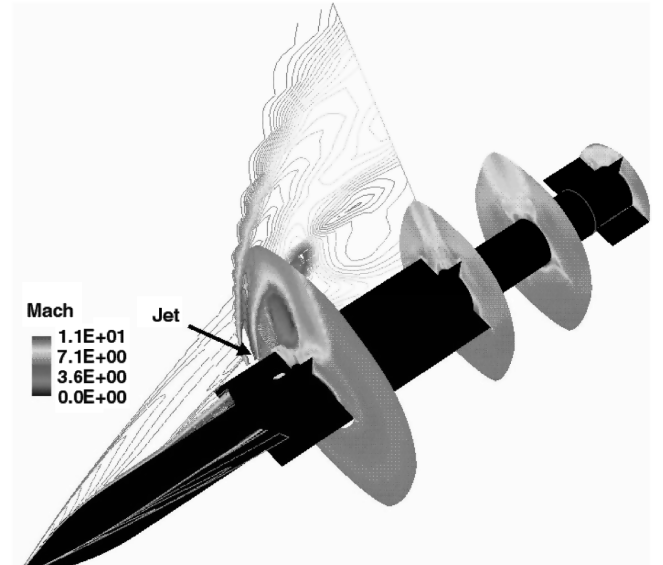


Fig. 5 Mach number contours for 19.7-km altitude, jet-on case.

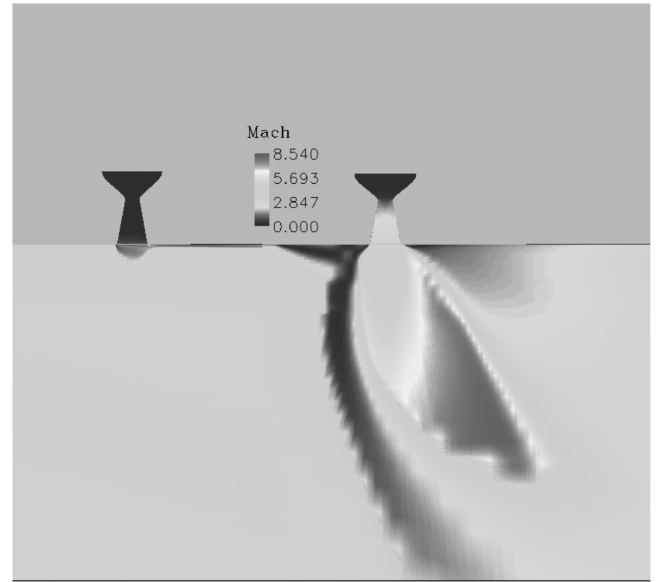


Fig. 6 Mach number contour for 19.7-km altitude, jet-on and -off cases.

and

$$C_M = M / 0.5 \rho_\infty V_\infty^2 A_{\text{ref}} L_{\text{ref}}$$

where F_x is a surface-integrated force component, M is a surface-integrated moment component, ρ_∞ is the freestream density, V_∞ is the freestream velocity, A_{ref} is a reference area, and L_{ref} is a reference length. For the purposes of this analysis, A_{ref} and L_{ref} are specified by the vehicle cross-sectional area and diameter, respectively. All moment calculations are performed with respect to a point on the vehicle centerline six calibers from the nose tip. This axial position corresponds to the center of the jet exit area.

In general, for the jet interaction problem, the total force acting on the body can be decomposed into three components: the aerodynamic force on the external body in the absence of the jet, the force produced at the jet exit location, and the aerodynamic interaction force produced by the jet interaction with the external flowfield. The force produced at the jet exit results from a

Table 2 Supersonic interceptor missile freestream conditions

Altitude, km	19.7
Flight Mach number	5.0
Static pressure, atm	0.57
Air density, kg/m ³	0.0938
Static temperature, K	216.67
Missile velocity, m/s	1475.0
Angle of attack, deg	0.0
Yaw angle, deg	0.0
Molecular weight (air)	28.967
Ratio of specific heats	1.4

Table 3 Jet interaction CFD cases

Case no.	Time integration	Divert-jet flow	Flow	Scale
1	Steady state	Off	Perfect	Full
2	Steady state	On	Perfect	Full
3	Steady state	Off	Perfect	1/10
4	Steady state	On	Perfect	1/10
5	Transient	On	Perfect	Full
6	Transient	Off	Perfect	Full
7	Steady state	On	Reacting	Full
8	Steady state	On	Frozen	Full

Table 4 Total computed force and moment coefficient

Case	Description	C_x	C_M	C_n
1	Full-scale, jet-off, perfect gas	0.260	—	—
	Percent relative to baseline case	-3.7	—	—
2	Full-scale, jet-on, perfect gas	0.270	0.855	0.54
	Baseline case	1	1	1
3	1/10 scale, jet-off, perfect gas	0.282	—	—
	Percent relative to baseline case	4.4	—	—
4	1/10 scale, jet-on, perfect gas	0.289	0.820	0.495
	Percent relative to baseline case	7.0	4.1	8.2
5	Full-scale, transient, jet on	0.258	0.997	0.651
	Percent relative to baseline case	-4.4	16.3	20.5
6	Full-scale, nonreacting, jet on	0.269	0.849	0.538
	Percent relative to baseline case	-0.3	-0.7	-0.37
7	Full-scale, reacting, jet on	0.257	0.758	0.615
	Percent relative to baseline case	-4.8	-11.3	13.8
	Percent relative to nonreacting	-4.4	-10.5	12.5

Table 5 Species inflow conditions

Jet species	Jet mole fraction	Freestream mole fraction
OH	0.006	0
O	0.007	0
H	0.009	0
C	0.08	0
CO	0.13	0
CO ₂	0.12	0
H ₂ O	0.21	0
O ₂	0.006	0.21
H ₂	0.25	0
HCl	0.10	0
N ₂	0.0001	0.79

combination of the momentum flux at the jet nozzle exit and the integrated pressure at the jet exit.

The relative magnitudes of the jet force and the jet interaction force can be compared through a jet interaction amplification factor K as shown in the following equation:

$$K = \frac{F_j + F_{JI}}{F_j}$$

where F_j is the force produced at the divert-jet exit and F_{JI} is the jet interaction force. Note that a positive value of F_{JI} indicates that the interaction force produces an effect that augments the jet force, F_{JI} . A negative value of F_{JI} indicates a reduction in the total force produced by the jet. An amplification factor greater than 1 indicates a favorable interaction between the jet and surrounding flow, that is, the disturbance of the vehicle pressure field by the jet is providing thrust augmentation. An amplification factor less than 1 indicates that the jet interaction force reduces the total force produced by the jet.

Comparisons of total computed forces and moment coefficients for all eight cases are summarized in Table 4. For each case, the induced normal force and pitching moment yield a center of pressure, that is, a pressure balance point, upstream of the jet exit center. All cases are compared to case 2, the baseline case, specified as full-scale geometry, jet on and perfect gas conditions. In Table 4, the values listed for the fin represent the combination of all dorsal and tail fins. The missile body carries the majority of the loads, roughly 80 to 90% of the axial force and 70% of the normal force and pitching moment. Furthermore, the fins handle the majority of the increase in the axial force as the divert jet is turned on. Comparisons of the geometric scale solutions indicate that matching the jet thrust coefficients for the difference scales (100 vs 10%) yield good agreement in predicted normal force, pitching moment, center of pressure, and force amplification factors. Force amplification factors of approximately 1.2 are predicted for each geometric scale. Overall, operation of the jet thruster induces a small increase in the axial force, a positive normal force in the direction of the jet thrust, and a positive pitching moment, causing the missile nose to pitch downward. The percent changes, relative to the baseline values for axial and normal forces and moment coefficients are shown in Table 4. For the jet-off solutions, only the axial force comparison is shown (3.7%). For geometric scale comparisons, the one-tenth scale solutions with the jet off and the jet operating were compared to the baseline case. The percentage differences for the axial and normal force coefficients and moment coefficients are relatively small. A difference of 4.1% is noted when comparing the pitching moments for the jet-on geometric scales, cases 2 and 4. The increased pitching moment is expected when comparing the one-tenth scale to the full-scale results because the most sensitive parameters of the forces and moments are magnified by a small (one-tenth geometric scale) of case 4. Differences noted in comparisons of the integrated normal force and pitching moment between the full-scale transient case and the baseline case are large. The large differences suggest strong transient influences on the normal force and pitching moment which cannot be ignored in the computational analysis for jet interaction. These pressures are higher than the steady-state pressure values because of the moving shock resulting from the JI phenomena. Comparison of reacting and nonreacting cases (case 7 versus case 8) shows noticeable external combustion effects on the integrated normal force and pitching moment.

The total fin and body-alone force and moment coefficients area are also provided in Table 4 for each case. The individual component of forces for each section in the missile is not included in Table 4.

Figures 7 and 8 include computed results of the transient JI solution at 19.7-km altitude and show the effects of the divert-jet startup process. Several transient time slices are shown, culminating in steady-state flow. Figure 7 depicts calculated transient static pressure contours on the surface of the interceptor vehicle from initiation of the divert-jet flow at $t = 0.0$, to established steady-state flow after approximately 6 ms. The results include the impingement of the interaction flow region on the dorsal fins at 3.5 ms.

Transient Mach number contours in the missile pitch plane are shown in Fig. 8 over the same time span. These results clearly illustrate the development of the jet shock structure and associated high pressures and low Mach numbers on the missile surface in the recirculation zone located upstream of the divert-jet exit position. The downstream expansion regions are characterized by supersonic flow and decreasing pressure. At higher altitude freestream conditions, the divert jet exhibits a greater plume expansion region and the divert-jet penetration distance also increases as the altitude increases [5]. A small disturbance at the divert-jet location is

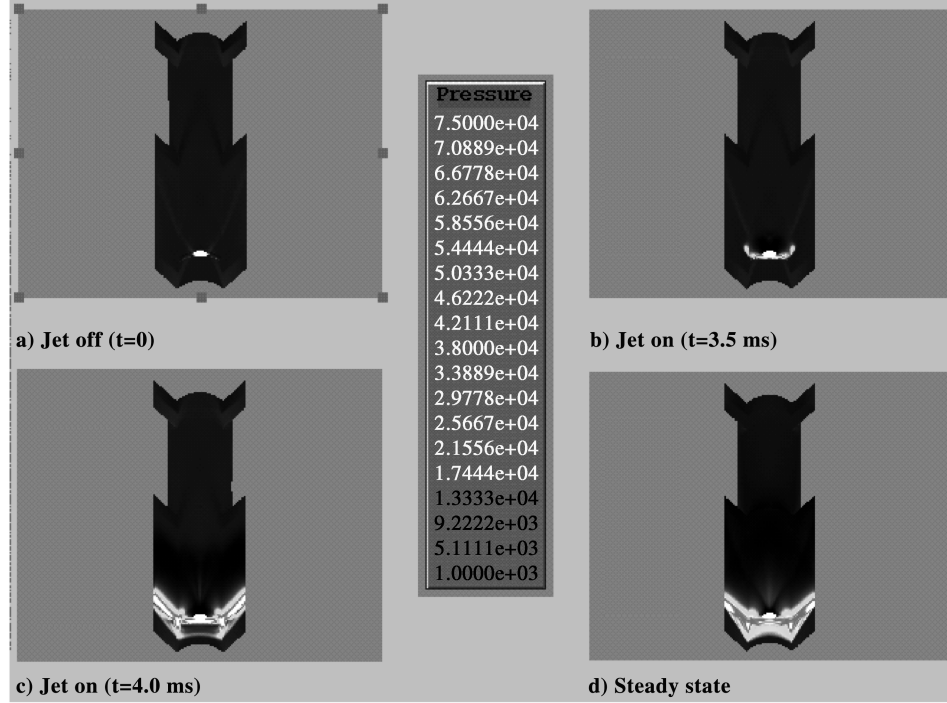


Fig. 7 Surface pressure at 19.7-km altitude, jet startup transient process.

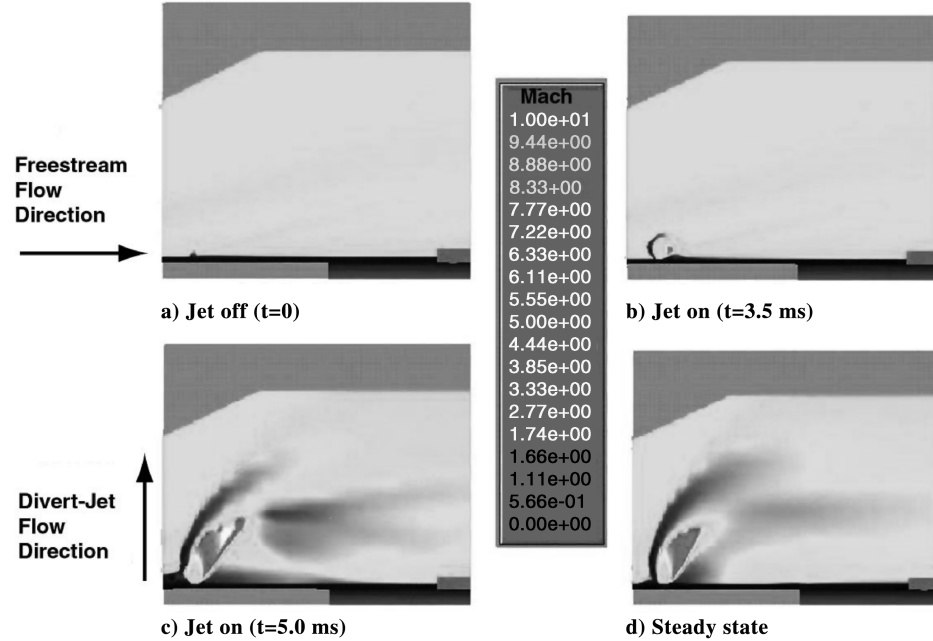


Fig. 8 Mach number contours for 19.7-km altitude, jet startup transient process.

apparent at $t = 0.0$ in Figs. 7 and 8. This disturbance results from the presence of the nozzle cavity before the initialization of the divert-jet flow.

The normal forces and pitching moments calculated over a complete divert-jet cycle, spanning the transient jet startup, steady-state, and transient shutdown process are presented in Figs. 9 and 10. As shown in Fig. 9, at time = 0 ms, the jet is turned on and the force rises abruptly, reaching a value of approximately 920 N. This force is attributed to the jet thrust alone. The force continues to rise as a high-pressure recirculation region develops and covers increasing areas of the cylindrical missile body.

The enhanced transient effect begins at approximately 2.6 ms, creating a body normal force in excess of 3300 N after 3.8 ms. A steady-state condition is established after 6 ms. The steady-state

force is approximately 1750 N which is greater than the magnitude of the jet force alone (920 N). As seen in Fig. 10, the pitching moment (computed about the center of the divert jet) quickly rises to a value of 550 N · m as the jet is turned on and appears to remain steady over the time period from 0 to 2.8 ms. At 2.8 ms, the pitching moment begins to increase approaching 2800 N · m after 4.5 ms. Recall that the JI region impinges on the dorsal fins of the missile after 4 ms. The effect of this impingement is evident in Figs. 9 and 10. Although the normal force reaches a maximum after 3.8 ms, the pitching moment continues to rise for another 0.7 ms. This delay in the maximum value of pitching moment is attributed to the impingement of the JI region on the dorsal fins creating further change in moment with little change in force. After 4.0 ms, the high-pressure region established in front of the divert jet continues to travel upstream, causing a slight

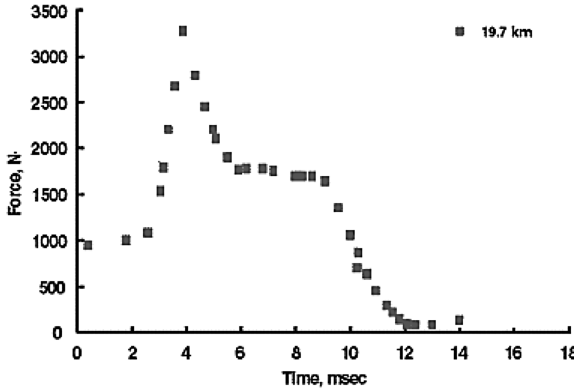


Fig. 9 Integrated normal force from start to shutdown at 19.7 km.

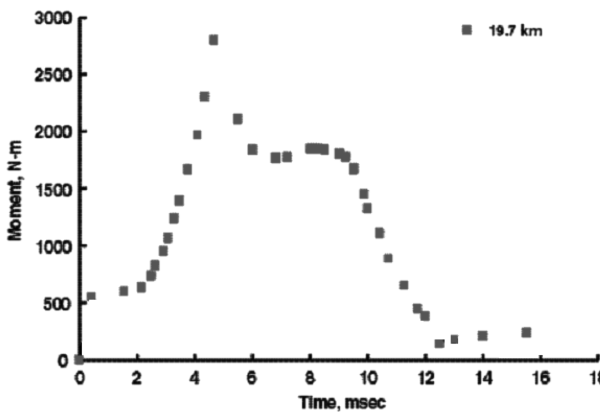


Fig. 10 Integrated pitching moment from start to shutdown at 19.7 km.

drop in surface pressure and pitching moment as the moving shocks become more stationary and oblique to the oncoming freestream flow. Although a net decrease in the normal force and pitching moment results from the separation region acting on the missile, the resulting steady-state force equal to 1750 N is almost double the force value computed for the divert jet alone, equal to 920 N. The resulting steady-state pitching moment equal to 1800 N·m is a factor of 3 greater than the pitching-moment value computed for the divert jet alone, equal to 550 N·m.

The transient spike occurs in the startup process at 3.5 ms. As discussed in the author's previous paper [5], the transient spike and the JI impingement on the dorsal fins occur earlier in the transient startup process as the altitude increases and the associated freestream static pressure decreases. Therefore, the delay in the maximum value of the pitching moment is predicted to be of longer duration as the altitude increases. The peak transient interaction force at a higher altitude condition is considerably less when compared with the peak transient interaction force at lower altitudes. This difference is attributed to the lower ambient pressures at the higher altitude freestream static conditions.

After the divert jet shuts down, the force and moment begin to decrease. The normal force appears to remain steady for approximately 1.1 ms as the flowfield adjusts to the new condition. The moment, shown in Fig. 10, also appears to experience a delayed response to the jet shutdown and begins to decrease after a period of approximately 1.5 ms. The final jet-off, steady-state force is equal to approximately 80 N, and the moment is equal to 120 N·m. Because of the presence of the jet cavity, the jet-off flowfield is not axisymmetric. The shutdown process requires approximately 4.5 ms to achieve steady-state conditions.

CFD results such as these can be used to assess interceptor missile reaction times as well as aerodynamic influences afforded by the operation of the divert jet. These results also indicate that CFD techniques can be applied to optimize the geometric configurations of integrated divert-jet, missile-interceptor design features. CFD can

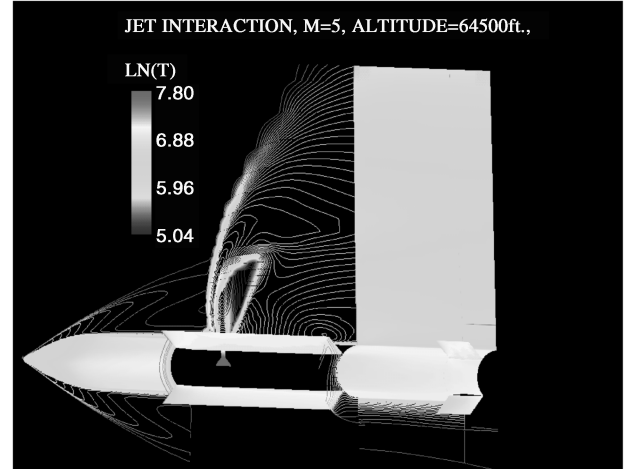


Fig. 11 Temperature contours for reacting flow calculation.

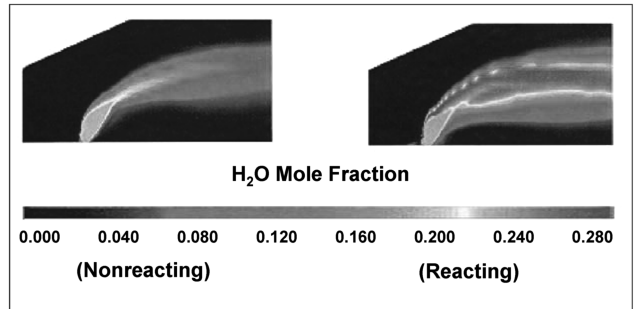


Fig. 12 Comparison of reacting and nonreacting H_2O mole fraction contours.

be applied to gain insight into the JI region, including enhancement effects of the JI separation region. Knowledge of the origin of these effects can be applied to ensure stable missile aerodynamics. Furthermore, these calculations strongly suggest that the transient effects predicted when the JI separation region impinges on the missile dorsal fin could have an influence on the aerodynamic behavior of the missile and should be carefully considered in the overall design analysis. Detailed transient CFD calculations completed for several cases are discussed in [5].

In the steady-state, finite-rate combustion CFD simulations, 14 chemical species and 46 reactions are considered. The species inflow condition is shown in Table 5. The CFD solution including finite-rate combustion is contrasted with a CFD solution assuming frozen chemistry to determine the effects of divert-jet exhaust plume combustion on the missile aerodynamic performance. The CFD investigation of the combustion effects assumes steady-state conditions. The comparison between reacting and frozen flow solutions indicated the recirculation region upstream of the jet is slightly larger in the reacting flow conditions when compared with the size of the recirculating region predicted in the nonreacting, frozen condition. The reacting exhaust plume chemistry includes noticeable hydrogen–oxygen combustion [10]. As expected, the exothermic combustion results in higher gas temperatures, when compared with the temperatures predicted for the frozen assumption. The temperature contours for the reacting flow case are shown in Fig. 11. A comparison of H_2O mole fraction in the symmetry plane of the missile for both reacting and nonreacting cases is shown in Fig. 12. Figure 12 clearly shows that H_2O production is greater in the reacting cases due to the combustion of H_2 fuel with oxygen present in the freestream air. In the nonreacting cases, changes in the H_2O mole fractions note in the exhaust plume interaction region are due solely to convection and diffusion. As noted in the H_2O mole fractions comparison, reacting vs frozen, the combustion process is somewhat limited in this application. The results of the force and

moment calculations were compared for the nonreacting and reacting case solutions. The pressure field for reacting and frozen cases was integrated over the vehicle surface to determine the forces and moments. The force and moment coefficients were computed for both cases and compared. These calculations indicate that external burning in the divert-jet exhaust will produce a small but noticeable effect on the forces and moments experienced by the vehicle.

The jet amplification factors for the reacting and nonreacting cases are 1.259 and 1.198, respectively. The reacting solution results in a thrust amplification factor that is 4.8% greater than the corresponding thrust amplification factor determined for the nonreacting frozen solution.

For the steady-state solutions, CFD convergence was determined by a 5-order-of-magnitude reduction in computed residuals and constant flowfield behavior. The transient computations were executed in a time-accurate RAN mode and required considerably longer CPU times compared to the steady-state solutions. Additionally, transient CFD analyses cannot take advantage of convergence acceleration techniques such as grid sequencing (solving for a solution on a coarse grid sequence and then interpolating the solution to a finer grid sequence is called mesh sequencing). To ensure an eventual steady-state condition, the transient cases were continued to 14 ms. The results indicate steady-state conditions were achieved at 6 ms.

V. Summary

CFD simulations of jet interaction flowfields were completed and contrasted to assess the effects of transient divert-jet operations, chemical combustion in the JI region, and geometric scale on the aerodynamic performance of a generic interceptor missile operating at supersonic flight conditions. Parametric computational fluid dynamic solutions were obtained at altitude conditions corresponding to 19.7 km for the following scenarios: 1) steady-state conditions with the lateral control jet turned off; 2) steady-state conditions with the lateral control jet turned on; 3) steady-state, full scale; 4) steady-state, one-tenth scale; 5) transient jet startup conditions; 6) transient jet shutdown conditions; 7) steady-state, finite-rate chemistry; and 8) steady-state frozen chemistry. The analyses include evaluation of flowfield phenomena as well as predicted missile surface pressures, normal forces, and pitching moments on generic interceptor missile geometry. The results indicate strong transient divert-jet effects occur which should be considered when designing control algorithms for pulsed-jet reaction control systems with short pulse times. These forces appear to be enhanced when the high-pressure separation region that forms in front of the divert jet impinges on the dorsal fins of the interceptor missile. The impingement pressures are much higher when compared with the steady-state pressure values because of the moving shock resulting from the JI phenomena. The duration of the transient effects is predicted to be approximately 3 to 6 ms after which the force begins to decay and approach steady-state values. The transient results indicate that the divert-jet shutdown process requires more time to reach steady-state conditions when compared with the jet startup process.

Steady-state CFD JI solutions were completed and compared assuming finite-rate chemistry and frozen chemistry conditions. Both solutions show similar flowfield phenomena, structure, and features. The reacting solutions indicates hydrogen–oxygen combustion occurs in the fuel-rich plume from the divert jet creating elevated temperatures and minimal force amplification, when compared with the frozen case.

This investigation demonstrates the utility of state-of-the-art CFD tools to address issues pertaining to complex flow interactions of interest in the propulsion arena today. These CFD calculations can provide an economical means to supplement the costly interceptor design and testing process and reduce development and testing resource requirements. CFD solutions can be applied to optimize the test matrices and evaluate candidate missile/divert-jet geometries and operating conditions and identify potential problem areas before production. The CFD flowfields can be analyzed to gain insight into the force amplification phenomena and to understand and properly account for the transient behavior and external combustion. The flowfield details calculated and visualized in this study cannot be measured in the harsh testing environments using modern flow visualization and measurement techniques.

The analysis predicts strong transient influences, noticeable external combustion influences, and very small full-scale vs one-tenth scale effects for the integrated normal force and pitching moment.

Additional CFD studies investigating the effects of multiphase chemistry in the interaction region are needed to complete the CFD feasibility demonstration.

Acknowledgment

This investigation was supported by the Ballistic Missile Defense Organization.

References

- [1] Srivastava, B., "Lateral Jet Control of a Supersonic Missile: CFD Predictions and Comparison to Force and Moment Measurements," AIAA Paper 97-0639, 6–9 Jan. 1997.
- [2] Chan, S. C., Roger, R. P., Edwards, G. L., and Brooks, W. B., "Integrated Jet Interactions CFD Predictions and Combustion to Force and Moment Measurements for a Thruster Attitude Controlled Supersonic Missile," AIAA Paper 93-3522, 1993.
- [3] Ebrahimi, H. B., "Validation Database for Propulsion Computational Fluid Dynamics," *Journal of Spacecraft and Rockets*, Vol. 34, No. 5, 1997, pp. 642–650.
- [4] Naumann, K. W., Ende, H., George, A., and Mathieu, G., "Stationary and Time-Dependent Effect in Near Interaction of Gaseous Jets and Supersonic Cross Flow," AIAA Paper 98-2972, June 1998.
- [5] Ebrahimi, H. B., "Numerical Simulation of Transient Jet Interaction Phenomenology in a Supersonic Freestream," *Journal of Spacecraft and Rockets*, Vol. 37, No. 6, Dec. 2000, pp. 713–719.
- [6] Ebrahimi, H. B., Levine, J., and Kawasaki, A., "Numerical Investigation of Twin-Nozzle Rocket Plume Phenomenology," *Journal of Propulsion and Power*, Vol. 16, No. 2, March 2000, pp. 178–186.
- [7] Ebrahimi, H. B., Rajendra, M., and Merkle, C. L., "Multi-Level Analysis of Pulsed Detonation Engines," *Journal of Propulsion and Power*, Vol. 18, No. 2, March 2002, pp. 225–232.
- [8] Yeneriz, M. A., and Davis, J. C., "Comparison of Calculation and Experiment for a Lateral Jet from a Hypersonic Biconic Vehicle," AIAA Paper 91-2097, July 1989.
- [9] Srivastava, B., "Computational Analysis and Validation for Lateral Jet Controlled Missiles," *Journal of Spacecraft and Rockets*, Vol. 34, No. 5, Sept.–Oct. 1997, pp. 584–592.
- [10] Robinson, Michael, A., "Application of CFD to BMDO JI Risk Mitigation: External Burning," AIAA Paper 99-0803, January 1999.

R. Cummings
Associate Editor